

Origin of resolution enhancement by co-doping of scintillators: Insight from electronic structure calculations

Daniel Åberg,^{1, a)} Babak Sadigh,¹ André Schleife,² and Paul Erhart^{3, b)}

¹⁾Physical and Life Sciences Directorate, Lawrence Livermore National Laboratory, Livermore, California 94550, USA

²⁾Department of Materials Science and Engineering, University of Illinois at Urbana-Champaign, Urbana, Illinois 61801, USA

³⁾Chalmers University of Technology, Department of Applied Physics, Gothenburg, Sweden

It was recently shown that the energy resolution of Ce-doped LaBr₃ scintillator radiation detectors can be crucially improved by co-doping with Sr, Ca, or Ba. Here we outline a mechanism for this enhancement on the basis of electronic structure calculations. We show that (i) Br vacancies are the primary electron traps during the initial stage of thermalization of hot carriers, prior to hole capture by Ce dopants; (ii) isolated Br vacancies are associated with deep levels; (iii) Sr doping increases the Br vacancy concentration by several orders of magnitude; (iv) Sr_{La} binds to V_{Br} resulting in a stable neutral complex; and (v) association with Sr causes the deep vacancy level to move toward the conduction band edge. The latter is essential for reducing the effective carrier density available for Auger quenching during thermalization of hot carriers. Subsequent de-trapping of electrons from Sr_{La} – V_{Br} complexes then can activate Ce dopants that have previously captured a hole leading to luminescence. This mechanism implies an overall reduction of Auger quenching of free carriers, which is expected to improve the linearity of the photon light yield with respect to the energy of incident electron or photon.

Scintillator radiation detectors have many applications in nuclear and radiological surveillance, high-energy physics, and medical imaging.^{1,2} The energy resolved detection of radiation is of particular interest as it enables for example the identification of fissile materials.³ According to counting statistics the resolution increases with luminosity, which usually results from a higher conversion efficiency, *i.e.*, relatively more photons are generated per incident energy. In practice the resolution is further limited by the non-linear response of the scintillator to the energy of the incident radiation.⁴ It is usually accepted that the resulting non-proportionality arises from the competition between non-radiative quenching, defect carrier trapping, as well as activator capture and subsequent emission.^{5–9}

One of the most promising materials for detector performance is Ce-doped LaBr₃.¹⁰ It yields an energy resolution of 2.7% at a photon energy of 662 keV in combination with an extremely fast scintillation pulse. LaBr₃ has been very well characterized both experimentally¹¹ and theoretically.^{12–14} The prospect of improving energy resolution by co-doping LaBr₃:Ce with Sr or Ba was first noted experimentally by Yang *et al.*¹⁵ Later Alekhin *et al.* revisited this aspect and using Ca and Sr achieved an improvement of energy resolution down to 2.0% at 662 keV.¹⁶ A more comprehensive investigation including both the alkaline as well as earth-alkaline series revealed that better performance is only achievable when using the heavier elements of the latter series (Sr, Ca, Ba).^{17,18} Several possible mechanisms were tentatively proposed

to rationalize these observations:¹⁹ (i) reduction of the nonradiative recombination rate, (ii) an increase of the so-called escape rate of the carriers from the quenching region, or (iii) an increase in the trapping rate of Ce³⁺. Here we address this question via first principles calculations of thermodynamic and electronic properties of intrinsic and extrinsic defects as well as their complexes in Ce and Sr-doped LaBr₃. It is found that Br vacancies are present in LaBr₃ regardless of the chemical boundary conditions and are associated with a deep electronic level below the conduction band minimum (CBM). They bind to Sr, which is preferentially incorporated substitutionally on La sites. Upon complexation, the vacancy defect level moves closer to the CBM becoming more shallow. As trapping on lattice defects effectively reduces the free carrier density available for Auger quenching,²⁰ we argue that this trap is essential for the improved linearity of LaBr₃:Ce. Our analysis is supported by the identification of distinct optical signatures associated with Ce sites in close correspondence to recent measurements.¹⁹ The presence of less deep trap levels also provide a rationale for the experimentally observed longer life-times.¹⁹

Calculations were performed within density functional theory (DFT) using the projector augmented wave (PAW) method²¹ as implemented in the Vienna ab-initio simulation package.²² Exchange-correlation were treated within the generalized gradient approximation.²³ DFT+*U* type on-site potentials²⁴ were included for both La-4*f* ($U_{\text{eff}} = 10.3$ eV) and Ce-4*f* states ($U_{\text{eff}} = 1.2$ eV) in order to obtain the correct ordering of La-5*d* and 4*f* states and to reproduce experimental Ce-4*f* ionization energies.^{13,14,25} The plane-wave energy cutoff was set to 230 eV and Gaussian smearing with a width of 0.1 eV was used to determine the occupation numbers. Excited Ce-4*f*⁰ states were obtained in a similar, albeit more flex-

^{a)}Electronic mail: aberg2@llnl.gov

^{b)}Electronic mail: erhart@chalmers.se

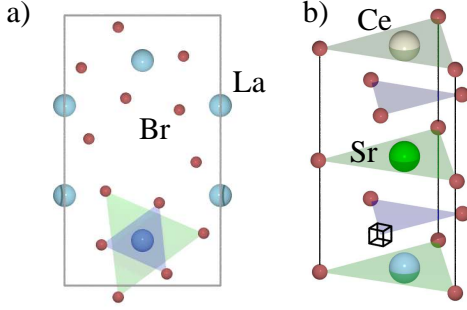


FIG. 1. (a) View along z -axis of the conventional LaBr_3 cell. (b) Strontium-vacancy defect cluster $\text{Sr}_{\text{La}} - \text{V}_{\text{Br}}$. The vacancy is illustrated by the hollow black box. For reference, we here also display one possible cerium site.

ible and automatized, approach as used by Canning and co-workers.¹³ First, a subspace of Ce-4*f* states was determined by projection of single particle wave functions on spherical harmonics within the PAW spheres. This is possible for localized atomic states, such as the rare-earth 4*f* states. The 4*f* occupation number can then be controlled by introducing a separate electron chemical potential for the subspace. Lanthanum bromide adopts a hexagonal lattice structure in space group 176 ($P6_3/m$) with La and Br ions occupying Wyckoff sites 2*c* and 6*h*, respectively. The calculated lattice parameters are $a = 8.140 \text{ \AA}$ and $c = 4.565 \text{ \AA}$ to be compared with experimental values of $a = 7.9648(5) \text{ \AA}$ and $c = 4.5119(5) \text{ \AA}$, respectively, see Fig. 1.²⁶ Defects were modeled using 168-atom supercells. Γ -point sampling was found to be sufficient to converge defect formation energies to better than 0.05 eV. Configurations were relaxed until ionic forces were less than 10 meV/ \AA . Defect formation energies were calculated using the formalism described in Refs. 27. Potential alignment as well as periodic image charge corrections were taken into account to correct for finite size effects.^{28,29} Defect concentrations were obtained using the calculated formation energies on the basis of a self-consistent solution of the charge neutrality condition 27 and 30.

In agreement with earlier calculations¹³ we find that in its ground state Ce preferentially substitutes for La with small distortions and adopts a neutral charge state corresponding to a $\text{Ce}^{3+} - 4f^1 5d^0$ configuration. By choice of the DFT+*U* parameters, the occupied 4*f* level is located 0.9 eV above the valence band maximum (VBM). The excited $\text{Ce} - 4f^0 5d^1$ state, which is obtained by enforcing the deoccupation of Ce-4*f* levels, is associated with the emergence of electronic levels very close to the CBM. They are predominantly of Ce-5*d* character and strongly hybridized with the neighboring La-5*d* states.

From an extensive exploration of intrinsic defects one obtains bromine vacancies V_{Br} to be the most energetically favorable donor-type defect under both La and Br-

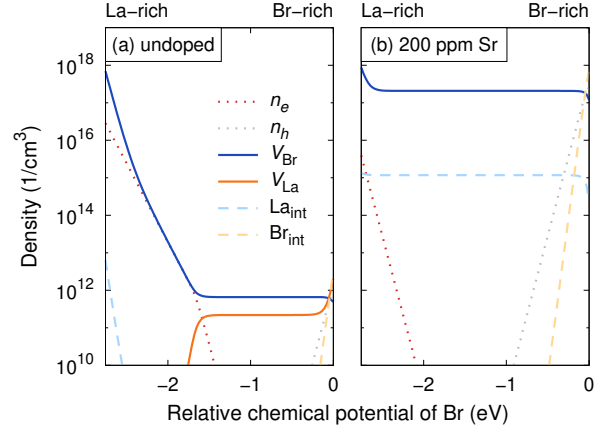


FIG. 2. Equilibrium defect and charge carrier concentrations as a function of the Br chemical potential at a temperature of 600 K. Results are shown both for (a) pure material and (b) LaBr_3 doped with 200 ppm Sr corresponding to the experimental doping conditions. Note that doping with Sr increases the Br vacancy concentration by several orders of magnitude. (Ce was not explicitly included in these figures since it does not affect the charge neutrality condition).

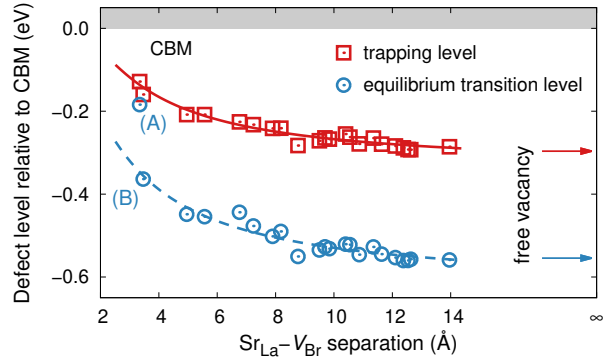


FIG. 3. Trapping and equilibrium transition levels for the (+1/0) transition of $\text{Sr}_{\text{La}} - \text{V}_{\text{Br}}$ as a function of $\text{Sr}_{\text{La}} - \text{V}_{\text{Br}}$ separation. The former was calculated by considering the transition level for fixed ionic positions starting from the $\text{V}_{\text{Br}}^\bullet$ configuration. The equilibrium transition level, on the other hand, was computed allowing full relaxation in both charge states. The data points labelled A and B indicate out-of-plane (A) and in-plane (B) configurations of nearest neighbor defect complexes, compare Fig. 1.

rich conditions, see Fig. 2(a). The Br vacancy is associated with an equilibrium transition level (+1/0) 0.55 eV below the conduction band minimum (CBM), see Fig. 3 and a trap state 0.3 eV below the CBM. The associated electronic level is located inside the band gap and has La-5*d* character. It can act as an efficient electron trap, effectively removing carriers from the light-generation process during the instrumentation pulse shape-time.

The inclusion of strontium is accomplished by substitution on lanthanum sites. The resulting $\text{Sr}_{\text{La}}^\bullet$ defect acts

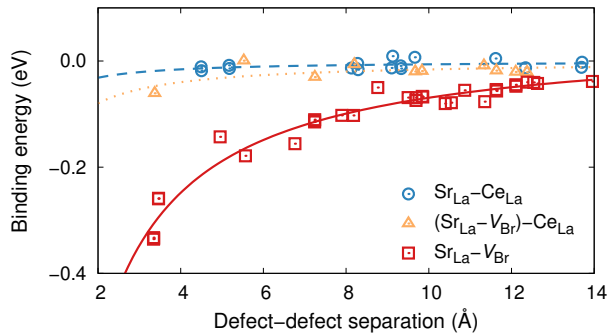


FIG. 4. Binding energy as a function of defect separation for various defect associates. While there is a strong attraction between V_{Br}^{\bullet} and Sr'_{La} , the interaction of $\text{Ce}_{\text{La}}^{\times}$ with other defects is weak. The variation in the binding energies is related to the anisotropy of the crystal structure.

as a shallow acceptor with a vanishingly small lattice distortion. Assuming a Sr concentration of 200 ppm the concentration of Br vacancies will increase by several orders of magnitude compared to pristine or Ce-only doped material as shown in Fig. 2. The opposite charge states of V_{Br}^{\bullet} and Sr'_{La} cause a mutual attraction, which is quantified in Fig. 4 revealing a binding energy of -0.3 eV for the nearest neighbor $(\text{Sr}_{\text{La}} - V_{\text{Br}})^{\times}$ complex³¹. See Fig. 1b for an example of complex geometry. A closer inspection of the electronic structure of the complex reveals that both the trap and equilibrium transition levels, which are associated with the Br vacancy, shift closer to the CBM by approximately 0.2 eV compared to the isolated vacancy, see Fig. 3.

The shift of the defect level can be rationalized by considering that Sr'_{La} introduces a point charge-like electrostatic potential that shifts the *local* energy scale. Localized states such as the V_{Br} defect level are sensitive to this shift whereas the delocalized states that make up the valence and conduction bands are unaffected, causing an effective upward shift of the vacancy level.

We can now consider the effect of the $\text{Sr}_{\text{La}} - V_{\text{Br}}$ complex on the electronic structure of Ce_{La} . Even though the binding between Ce_{La} and $\text{Sr}_{\text{La}} - V_{\text{Br}}$ is weak as shown in Fig. 4, the large concentration of Ce (5%) used experimentally^{15,32} implies that the average separation between Ce_{La} and $\text{Sr}_{\text{La}} - V_{\text{Br}}$ is only about 2.5 unit cells. As a result, each $\text{Sr}_{\text{La}} - V_{\text{Br}}$ complex will have a Ce atom in its vicinity. One can thus expect the spectroscopic signatures of cerium in Sr-doped $\text{LaBr}_3\text{:Ce}$ to be affected. To this end we have calculated Ce ($4f \leftrightarrow 5d$) excitation and emission energies for isolated Ce_{La} as well for various complexes of Ce_{La} with $\text{Sr}_{\text{La}} - V_{\text{Br}}$, where the latter are nearest neighbors. Spin-orbit interaction was not included self-consistently but rather added as a perturbation to the $4f$ states according to

$$\Delta E_{\text{so}} = \begin{cases} -2\xi_{4f} & j = 5/2 \\ 3/2\xi_{4f} & j = 7/2, \end{cases}$$

TABLE I. Comparison of calculated and experimental data for Ce excitation and emission ($4f^1 5d^0 \leftrightarrow 4f^0 5d^1$). Values in brackets in the excitation column indicate the shift with respect to free Ce_{La} , which is identical to site I in the case of the experimental data. Two values are given in the emission column corresponding to final states of $^2F_{5/2}$ and $^2F_{7/2}$, respectively. Experimental data from Ref. 19. Note that the band gap error of DFT manifests itself in a systematic underestimation of all excitation and emission energies.

Site	Excitation (eV)	Emission (eV)	Stokes shift (eV)
Calculation			
Ce_{La}	3.56	3.13 / 2.78	0.43
$(\text{Sr}_{\text{La}} - V_{\text{Br}}) - \text{Ce}_{\text{La}}$	3.22 (−0.34)	2.78 / 2.43	0.31
Experiment (Ref. 19)			
I	4.03	3.47 / 3.19	0.56
II	3.59 (−0.44)	3.36 / 3.10	0.24
III	3.47 (−0.56)	3.27 / 3.10	0.21

where $\xi_{4f} = 0.1$ eV as obtained from the $4f$ splitting in a $\text{Ce-}4f^0 5d^1$ configuration.

The thus obtained optical signatures can be categorized as follows (also compare Table I): Isolated Ce is associated with the largest excitation energy and a substantial Stokes shift. For configurations, in which the Br vacancy is a *first neighbor* of Ce a pronounced reduction of both excitation and emission energies is observed with a typical value of -0.34 eV given in Table I. Furthermore the Stokes shift is reduced compared to isolated Ce. There are several configurations with similar optical signatures. Given the accuracy that can be expected from the present DFT calculations, however, we abstain from a more detailed differentiation of these complexes and in Table I only include the results for a representative cluster. Finally, configurations, for which Ce and V_{Br} are *not* first nearest neighbors behave similar to isolated Ce.

We now wish to point out several important facts. Firstly, we note that the shift in the calculated excitation energy (0.34 eV) between Ce_{La} and $(\text{Sr}_{\text{La}} - V_{\text{Br}}) - \text{Ce}_{\text{La}}$ is close to the experimental shift between sites I and II/III ($0.44/0.56$ eV). Thus we associate site I with Ce_{La} and II/III with nearest neighbor triple complexes. Since Ce is a nearest neighbor of a Br vacancy in these configurations, the deep trap level associated with the vacancy will to a large part consist of $\text{Ce-}5d$ states. This explains, the reduction of the excitation energy for this complex compared to isolated Ce_{La} . Furthermore, if we assume the $4f$ level to be unaffected by the neutral complex $\text{Sr}_{\text{La}} - V_{\text{Br}}$, it implies that we can identify the shift in excitation energy with the trap depth.

To summarize, we demonstrated that co-doping of $\text{LaBr}_3\text{:Ce}$ with strontium gives rise to a shallow acceptor substituting on a lanthanum site. Overall charge neutral-

ity requires formation of one oppositely charged bromine vacancy for each strontium atom, resulting in a steep increase of Br concentration compared to the undoped material. Moreover, the two defects are electrostatically attracted to each other and will form stable complexes that act as electron traps. We note that neutral Ce atoms are not likely to capture electrons, since the $5d$ states in this case are situated inside the conduction band.¹³ The occupied Ce $4f$ level is located rather deep inside the gap (0.6–0.9 eV) and will therefore have a low but finite hole capture rate. If we assume that Ce is activated by sequential capture of a hole and electron this implies that hole capture is the rate limiting step. Since Auger recombination, which has been shown to be the major quenching channel at this time scale for halide scintillators,²⁰ has a cubic dependence on the electron and hole densities the carrier population will be greatly reduced by non-linear quenching causing an overall non-proportional response. If, however, $\text{Sr}_{\text{La}} - V_{\text{Br}}$ traps are active during the initial thermalization stage (2–10 ps in halide systems) they will effectively reduce the free electron density. As a result, a larger density of holes will remain available for ionization of cerium activators without being quenched by the Auger mechanism. Although calculation of electron capture cross-sections for the complexes are beyond the scope of this letter, we note that a very fast capture is indeed possible. For example, in picosecond optical absorption experiments it is shown that energy transfer to europium activators in $\text{SrI}_2\text{:Eu}$ may be as fast as 400 fs.³³

Another time-scale of importance is the de-trapping rate from the Br-vacancy sites. As alluded to earlier, each defect complex will be in close proximity to a Ce atom. Once any of the nearby Ce atoms captures a hole, Coulombic attraction serves as a driving force for transferring the electron from the complex to the activator. This suggests that non-linear quenching is reduced at the cost of longer decay-times; in fact, two of the three cerium sites discussed by Alekhin are associated with very long decay times ranging from 60–2500 ns while accounting for 20–45 % of the total light output.¹⁹

We acknowledge fruitful discussions with S. Payne, G. Bizarri, and R. T. Williams. This work was performed under the auspices of the U.S. Department of Energy by Lawrence Livermore National Laboratory under Contract DE-AC52-07NA27344 with support from the National Nuclear Security Administration Office of Non-proliferation Research and Development (NA-22). P.E. acknowledges funding from the *Area of Advance – Materials Science* at Chalmers. Computer time allocations by the Swedish National Infrastructure for Computing at NSC (Linköping) and C3SE (Gothenburg) are gratefully acknowledged.

¹P. A. Rodnyi, *Physical processes in inorganic scintillators* (CRC Press, Boca Raton, 1997).

²G. F. Knoll, *Radiation detection and measurement; 4th ed.* (Wiley, New York, NY, 2010).

- ³K. E. Nelson, T. B. Gosnell, and D. A. Knapp, *Nucl. Instrum. Methods A* **659**, 207 (2011).
- ⁴P. Dorenbos, *IEEE Trans. Nucl. Sci.* **57**, 1162 (2010).
- ⁵P. Dorenbos, *Phys. Status Solidi A* **202**, 195 (2005).
- ⁶A. V. Vasil'ev, *IEEE Trans. Nucl. Sci.* **55**, 1054 (2008).
- ⁷S. Kerisit, K. M. Rosso, B. D. Cannon, F. Gao, and Y. Xie, *J. Appl. Phys.* **105**, 114915 (2009).
- ⁸G. Bizarri, W. Moses, J. Singh, A. Vasilev, and R. Williams, *Journal of Luminescence* **129**, 1790 (2009), special Issue based on The 15th International Conference on Luminescence and Optical Spectroscopy of Condensed Matter (ICL'08).
- ⁹S. Payne, W. W. Moses, S. Sheets, L. Ahle, N. Cherepy, B. Sturm, S. Dazeley, G. Bizarri, and W.-S. Choong, *IEEE Trans. Nucl. Sci.* **58**, 3392 (2011).
- ¹⁰E. V. D. van Loef, P. Dorenbos, C. W. E. van Eijk, K. Krämer, and H. U. Güdel, *Appl. Phys. Lett.* **79**, 1573 (2001).
- ¹¹P. Dorenbos, E. V. D. van Loef, A. P. Vink, E. van der Kolk, C. W. E. van Eijk, K. W. Krämer, H. U. Güdel, W. M. Higgins, and K. S. Shah, *J. Luminescence* **117**, 147 (2006); F. P. Doty, D. McGregor, M. Harrison, K. Findley, and R. Polichar, *Proc. SPIE* **6707**, 670705 (2007).
- ¹²G. Bizarri and P. Dorenbos, *Phys. Rev. B* **75**, 184302 (2007); D. J. Singh, *ibid.* **82**, 155145 (2010).
- ¹³A. Canning, A. Chaudhry, R. Boutchko, and Grønbech-Jensen, *Phys. Rev. B* **83**, 125115 (2010).
- ¹⁴D. Åberg, B. Sadigh, and P. Erhart, *Phys. Rev. B* **85**, 125134 (2012).
- ¹⁵K. Yang, P. Menge, J. Buzniak, and V. Ouspenski, in *Nuclear Science Symposium and Medical Imaging Conference (NSS/MIC), 2012 IEEE* (2012) pp. 308–311.
- ¹⁶M. S. Alekhin, J. T. M. de Haas, I. V. Khodyuk, K. W. Krämer, P. R. Menge, V. Ouspenski, and P. Dorenbos, *Appl. Phys. Lett.* **102**, 161915 (2013).
- ¹⁷P. Dorenbos, M. Alekhin, I. V. Khodyuk, J. T. M. de Haas, and K. Krämer (Presented at SCINT 2013, Shanghai, China, 2013).
- ¹⁸M. S. Alekhin, D. A. Biner, K. W. Krämer, and P. Dorenbos, *J. Appl. Phys.* **113**, 224904 (2013).
- ¹⁹M. S. Alekhin, S. Weber, K. W. Krämer, and P. Dorenbos, *Journal of Luminescence* **145**, 518 (2014).
- ²⁰J. Q. Grim, K. B. Ucer, A. Burger, P. Bhattacharya, E. Tupitsyn, E. Rowe, V. M. Buliga, L. Trefilova, A. Gektin, G. A. Bizarri, W. W. Moses, and R. T. Williams, *Phys. Rev. B* **87**, 125117 (2013).
- ²¹P. E. Blöchl, *Phys. Rev. B* **50**, 17953 (1994); G. Kresse and D. Joubert, *ibid.* **59**, 1758 (1999).
- ²²G. Kresse and J. Hafner, *Phys. Rev. B* **47**, 558 (1993); **49**, 14251 (1994); G. Kresse and J. Furthmüller, **54**, 11169 (1996); *Comput. Mater. Sci.* **6**, 15 (1996).
- ²³J. P. Perdew, K. Burke, and M. Ernzerhof, *Phys. Rev. Lett.* **77**, 3865 (1996), erratum, *ibid.* **78**, 1396(E) (1997).
- ²⁴S. L. Dudarev, G. A. Botton, S. Y. Savrasov, C. J. Humphreys, and A. P. Sutton, *Phys. Rev. B* **57**, 1505 (1998).
- ²⁵M. T. Czyżyk and G. A. Sawatzky, *Phys. Rev. B* **49**, 14211 (1994).
- ²⁶K. Krämer, T. Schleid, M. Schulze, W. Urland, and G. Meyer, *Zeitschr. Anorg. Allg. Chemie* **575**, 61 (1989).
- ²⁷S. B. Zhang and J. E. Northrup, *Phys. Rev. Lett.* **67**, 2339 (1991); P. Erhart, D. Åberg, and V. Lordi, *Phys. Rev. B* **81**, 195216 (2010).
- ²⁸G. Makov and M. C. Payne, *Phys. Rev. B* **51**, 4014 (1995).
- ²⁹S. Lany and A. Zunger, *Phys. Rev. B* **78**, 235104 (2008).
- ³⁰P. Erhart and K. Albe, *J. Appl. Phys.* **104**, 044315 (2008).
- ³¹We here adopt the convention that negative binding energies indicate attraction.
- ³²M. S. Alekhin, J. T. M. de Haas, I. V. Khodyuk, K. W. Krämer, P. R. Menge, V. Ouspenski, and P. Dorenbos, *Appl. Phys. Lett.* **102**, 161915 (2013).
- ³³K. B. Ucer, G. Bizarri, A. Burger, A. Gektin, L. Trefilova, and R. T. Williams, *Phys. Rev. B* **89**, 165112 (2014).